ACS OMEGA

http://pubs.acs.org/journal/acsodf

Article

Elucidation of the Effect of Phospholipid Charge on the Rate of Insulin Aggregation and Structure and Toxicity of Amyloid Fibrils

Mikhail Matveyenka,[‖] Stanislav Rizevsky,[‖] and Dmitry Kurouski*

Cite This: *ACS Omega* 2023, 8, 12379−12386

Read Online

ACCESS | Metrics & More | Article Recommendations

ABSTRACT: The plasma membrane is a dynamic structure that separates the cell interior from the extracellular space. The fluidity and plasticity of the membrane determines a large number of physiologically important processes ranging from cell division to signal transduction. In turn, membrane fluidity is determined by phospholipids that possess different charges, lengths, and saturation states of fatty acids. A growing body of evidence suggests that phospholipids may play an important role in the aggregation of misfolded proteins, which causes pathological conditions that lead to severe neurodegenerative diseases. In this study, we investigate the role of the charge of the most abundant phospholipids in the plasma membrane: phosphatidylcholine and phosphatidylethanolamine, zwitterions: phosphatidylserine and phosphatidylglycerol, lipids that possess a negative charge, and cardiolipin that has double negative charge on its polar head. Our results show that both zwitterions strongly inhibit insulin aggregation, whereas negatively charged lipids accelerate fibril formation. We also found that in the equimolar presence of zwitterions insulin yields oligomers that exert significantly lower cell toxicity compared to fibrils that were grown in the lipid-free environment. Such aggregates were not formed in the presence of negatively charged lipids. Instead, long insulin fibrils that had strong cell toxicity were grown in the presence of such negatively charged lipids. However, our results showed no correlation between the charge of the lipid and secondary structure and toxicity of the aggregates formed in its presence. These findings show that the secondary structure and toxicity are determined by the chemical structure of the lipid rather than by the charge of the phospholipid polar head.

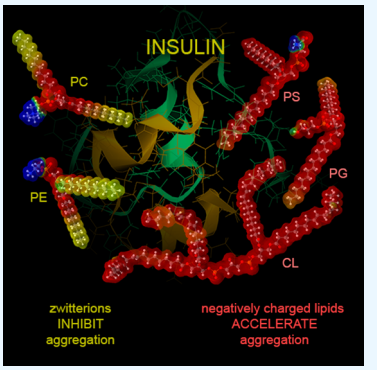

Downloaded via TEXAS A&M UNIV COLG STATION on June 12, 2023 at 13:51:21 (UTC).
See https://pubs.acs.org/sharingguidelines for options on how to legitimately share published articles.

INTRODUCTION

The plasma membrane separates the cell from the outside environment and regulates the transport of ions and molecular species, as well as cell endo- and exocytosis.[1,2] These critically important functions are determined by a fine balance of several classes of molecular species that include lipids, proteins, and carbohydrates.[3] A vast majority of lipids present in the plasma membrane are phospholipids. These molecules have two fatty acids (FAs) with different lengths of carbon atoms and a degree of saturation at sn-2 and sn-3 positions, whereas the sn-1 position of glycerol is occupied by a polar headgroup.[3,4] Depending on the charge possessed by the headgroup, all phospholipids can be divided into two main classes: zwitterions and anionic lipids.[5,6]

Zwitterionic lipids occupy around 75% of the lipid bilayer.[7] These molecular species determine membrane fluidity and permeability to hydrophobic molecules, such as steroid hormones.[3,8] Although negatively charged (anionic) lipids constitute significantly smaller volume of the plasma membrane, these molecules perform critically important functions in signal transition and cell apoptosis.[5,6] For instance, phosphatidylserine (PS) is an anionic lipid that is localized on the interior membrane of cells via ATP-dependent flippase transport.[1,4,9] An exposure of PS on the exterior part of the plasma membrane indicates cell malfunction.[10] In such cases, PS is recognized by phagocytes that degrade such apoptotic and necrotic cells.[3]

A growing body of evidence suggests that amyloid-associated proteins, such as amyloid β peptide, α-synuclein (α-syn), islet amyloid precursor protein (IAPP), and insulin can interact with phospholipids.[11−13] Such interactions drastically change the stability of amyloidogenic proteins, accelerating or decelerating their assembly into oligomers and fibrils. The high toxicity of these protein aggregates points to their strong connection to a large number of neurodegenerative diseases, including Alzheimer and Parkinson diseases.[14−16] Recently reported results by Dou and co-workers show that lipids not only altered the rates of α-syn aggregation but also drastically changed the secondary structure of α-syn oligomers.[17] Similar results were also reported by Rizevsky and co-workers.[18] Using

Received: January 9, 2023
Accepted: February 14, 2023
Published: March 21, 2023

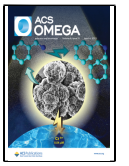

ACS Publications

© 2023 The Authors. Published by American Chemical Society

nanoinfrared spectroscopy, also known as atomic force microscopy infrared (AFM-IR) spectroscopy, the researchers demonstrated that insulin strongly interacts with both phosphatidylcholine (PC) and cardiolipin (CL). In AFM-IR, a metallized scanning probe is placed on the sample of interest.[19−21] Next, the sample is illuminated by pulsed tunable IR laser, which induces thermal expansions in the sample.[22−31] These expansions are recorded by the probe and converted into IR spectra.[18,19,32−35] Thus, AFM-IR can be used to determine the chemical structure of individual protein aggregates.[26−31,33−37] Using AFM-IR, Rizevsky and co-workers also found that both PC and CL were found to be present in insulin oligomers that were grown in the presence of these phospholipids.[18] Independently, Matveyenka and co-workers demonstrated that the degree of saturation of FAs of both PC and CL plays an important role in insulin aggregation.[32] Specifically, CL with unsaturated FAs enhanced insulin aggregation strongly than its fully saturated analog. Finally, Matveyenka and co-workers showed that insulin oligomers that were grown in the presence of saturated CL and PC exerted significantly lower cell toxicity than the aggregates formed in the presence of unsaturated analogs of CL and PC.[32] These results helped to understand the role of saturation of FAs in the phospholipids. However, the role of the charge of the phospholipids remains unclear.

In this study, we investigate the effect of the charge of the phospholipids on bovine insulin aggregation. Abrupt aggregation of this hormone is observed upon injection amyloidosis and diabetes type 2. In the former case, injection of insulin, which is routinely performed for diabetes type 1, leads to a high local concentration of the hormone in the skin dermis.[38,39] This triggers protein assembly into oligomers and fibrils, highly toxic species, that may, in turn, trigger abrupt aggregation of other proteins present in cell media, such as serum amyloid A and lysozyme. This leads to the development of systemic amyloidosis.[40] In the latter case, an overproduction of insulin in pancreas causes its aggregation, which, similar to injection amyloidosis, can trigger irreversible aggregation of IAPP and other proteins present in pancreas.[41]

We monitored the rate of protein aggregation in the presence of equimolar concentrations of two zwitterionic lipids, PC and phosphatidylethanolamine (PE), as well as two anionic lipids, PS and phosphatidylglycerol (PG). Finally, the effect of these anionic lipids on the rate of insulin aggregation was compared to CL, a phospholipid that possessed two negative charges per one lipid molecule. We also analyzed morphologies and the secondary structure of insulin aggregates formed in the presence of these lipids and determined the toxicity that these species exert to mice midbrain N27 cells.[33]

RESULTS AND DISCUSSION

Effect of Lipid Charges on the Rate of Protein Aggregation. In a lipid-free environment, insulin aggregation exhibits a well-defined lag-phase (t_{lag} = 14.9 ± 0.5 h) that is followed by a rapid increase in the ThT intensity, which indicates the formation of protein aggregates (Figure 1). We found that PS and PG drastically shortened t_{lag} of insulin aggregation when present in equimolar concentrations with the protein. Specifically, Ins:PG t_{lag} was found to be 3.9 ± 0.8 h, whereas Ins:PS t_{lag} = 8.5 ± 0.7 h. We have also found that both PG and PS can uniquely alter the rate of insulin aggregation. We found that PG $t_{1/2}$ was 6.9 ± 0.6 h, whereas PS $t_{1/2}$ was 10.9 ± 0.5 h. It should be noted that insulin $t_{1/2}$ = 16.5 ± 0.6 h.

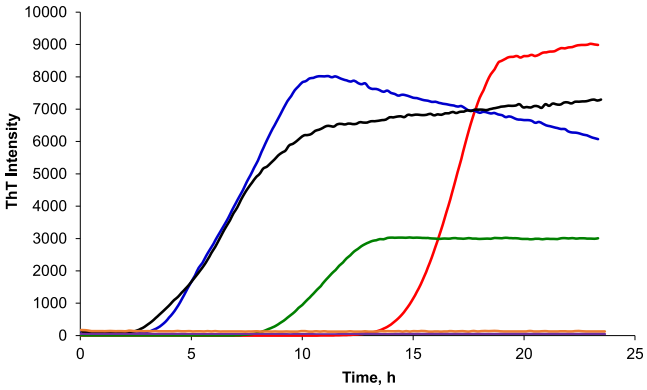

Figure 1. Negatively charged phospholipids drastically accelerate, whereas zwitterionic phospholipids strongly inhibit insulin aggregation. ThT aggregation kinetics of insulin in the lipid-free environment (red), as well as in the presence of PG (blue), PS (green), CL (black), PC (purple), and PE (orange). Each kinetic curve is the average of three independent measurements. For Ins, 400 μM of bovine insulin was dissolved in 1× phosphate-buffered saline (PBS) with 2 mM of ThT; pH adjusted to pH 3.0. For Ins:PG, Ins:PS, Ins:PS, Ins:CL, and Ins:PE, 400 μM of bovine insulin was mixed with an equivalent concentration of the corresponding lipid; pH was adjusted to pH 3.0. All samples were kept at 37 °C under 510 rpm for 24 h.

Thus, both PG and PS shortened the t_{lag} of insulin aggregation that accelerated the rate of fibril formation. It should be noted that CL (net charge −2) exerted a similar effect to PG and PS on the lag-phase and rate of insulin aggregation. In the equimolar presence of CL, insulin t_{lag} was found to be 3.8 ± 0.5 h, whereas $t_{1/2}$ was 6.5 ± 0.5 h.

We also found that the ThT intensity of insulin aggregation in the lipid-free environment is the highest compared to the intensities of ThT signals for Ins:PS, Ins:PG, and Ins:CL. This finding suggests that insulin aggregation in the presence of negatively charged lipids yields fewer ThT active protein aggregates. However, it should be noted that ThT affinity to amyloid aggregates, which ultimately correlates with the intensity of ThT fluorescence, can be affected by the hydrophobic/hydrophilic properties of such aggregates. Therefore, the above discussed difference in the ThT intensity of different protein samples cannot be unambiguously used for quantification of the concentration of amyloid aggregates.

ThT analysis of insulin aggregation in the presence of zwitterionic lipids showed that both PC and PE strongly inhibited fibril formation. Specifically, we observed no changes in the ThT signal over the course of 24 h. These findings show that no fibril formation takes place if insulin is exposed to equimolar concentrations of zwitterionic lipids.

Morphological Analysis of Protein Aggregates Formed in the Presence of Lipids and in the Lipid-Free Environment. Using AFM, we investigated the morphology of insulin aggregates grown in the presence of lipids, as well as in the lipid-free environment (Figure 2). We found that in the lipid-free environment (Ins), insulin formed long fibrils with a large distribution of lengths that were on average 12 nm in height (Figure 2). However, we observed no fibrils present in Ins:PC and Ins:PE. Instead, we found that insulin formed only small (4−6 nm in height) oligomers in the presence of zwitterionic lipids. This observation shows that zwitterionic lipids drastically alter the topology of insulin aggregates formed in their presence. AFM imaging also showed that in the presence of CL, PS, and PG, insulin aggregation

https://doi.org/10.1021/acsomega.3c00159
ACS Omega 2023, 8, 12379−12386

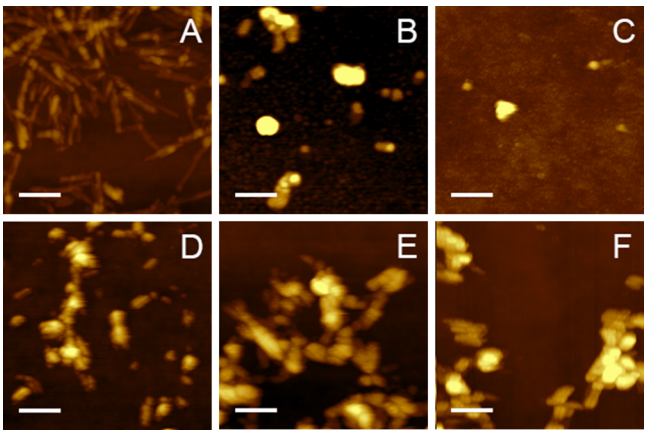

Figure 2. Zwitterionic phospholipids yield only oligomers (B, C), whereas negatively charged phospholipids produce short fibrils (D–F) when present in equimolar concentrations with insulin. AFM images of insulin fibrils grown in the lipid-free environment (A), as well as in the presence of PC (B), PE (C), PG (D), PS (E), and CL (F). Scale bars are 200 nm. For Ins, 400 μM of bovine insulin was dissolved in 1× PBS with 2 mM of ThT; pH adjusted to pH 3.0. For Ins:PG, Ins:PS, Ins:PS, Ins:CL, and Ins:PE, 400 μM of bovine insulin was mixed with an equivalent concentration of the corresponding lipid; pH was adjusted to pH 3.0. After 24 h of incubation of insulin (400 μM) with and without lipids at 37 °C under 510 rpm, sample aliquots were diluted with 1× PBS pH 3.0 and deposited onto precleaned silicon wafer.

yielded significantly shorter fibrils compared to those formed in the lipid-free environment. These aggregates were ∼200 nm long fibrils that were 6–8 nm in height. Finally, in addition to the fibrils, we found 30–60 nm spherical aggregates present in Ins:CL, Ins:PS, and Ins:PG. These findings show that negatively charged lipids significantly alter the morphologies of protein fibrils that form in their presence.

Elucidation of Protein Secondary Structure of Insulin Aggregates Grown in the Presence of Zwitterionic and Negatively Charged Lipids. We utilized AFM-IR to examine the secondary structure of insulin aggregates grown in the presence of zwitterionic and negatively charged lipids, as well as insulin fibrils that were formed in the lipid-free environment. This nanoscopy technique is based on laser-induced thermal expansions of the analyzed samples that are probed by the metalized scanning probe positioned above the sample of interest.[20,21,24,42,43] Thus, AFM-IR allows for a direct visualization of individual protein aggregates simultaneously enabling their structural analysis.[17,28,29,44]

AFM-IR spectra collected from insulin fibrils that were grown in the lipid-free environment (Ins) exhibit two vibrational bands in the amide I region of the spectrum that are centered around 1630 to 1668 cm^{-1}. It should be noted that 1630 cm^{-1} vibration had higher intensity than 1668 cm^{-1} band. These findings demonstrate that insulin fibrils grown in the lipid-free environment are dominated by parallel β-sheets with some unordered protein present in their secondary structure.[45,46] The same vibrational bands were evident in the AFM-IR spectra collected from Ins:PC oligomers. However, we observed the reversed ratio in the intensity of 1630 and 1668 cm^{-1} bands. This observation indicates that that Ins:PC oligomers consist of predominantly unordered proteins with some parallel β-sheets present in their secondary structure. We also found that AFM-IR spectra collected from Ins:PC exhibit intense vibrational bands around 800–900 cm^{-1}, 1000–1200 cm^{-1}, and 1730 cm^{-1}. These vibrational bands correspond to C–H, PO_2^- vibration, and C═O vibration of the ester group of lipids[44] (Figure 3). The presence of these vibrational bands in the AFM-IR spectra of Ins:PC points on the presence of PC in the structure of Ins:PC aggregates. Similar vibrational bands were observed in the AFM-IR spectra collected from Ins:PE oligomers. However, we found that intensity of 1000–1200 cm^{-1} (PO_2^-) bands was significantly lower than the intensity of these bands in the spectrum of Ins:PC. We also did not

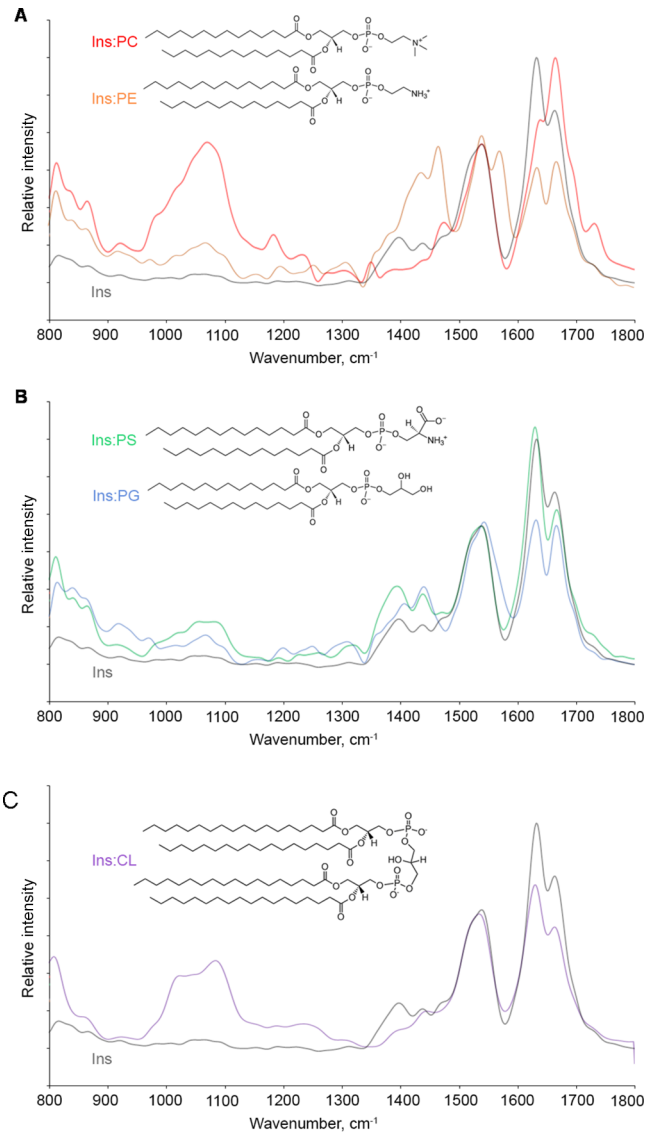

Figure 3. Nanoscale analysis of the secondary structure of insulin aggregates grown in the lipid-free environment and in the presence of phospholipids. Averaged AFM-IR spectra of (A) Ins (gray), Ins:PC (red), Ins:PE (orange); (B) Ins (gray), Ins:PS (green), Ins:PG (blue), (C) Ins (gray), and Ins:CL (purple) aggregates. For Ins, 400 μM of bovine insulin was dissolved in 1× PBS with 2 mM of ThT; pH adjusted to pH 3.0. For Ins:PG, Ins:PS, Ins:PS, Ins:CL, and Ins:PE, 400 μM of bovine insulin was mixed with an equivalent concentration of the corresponding lipid; pH was adjusted to pH 3.0. After 24 h of incubation of insulin (400 μM) with and without lipids at 37 °C under 510 rpm, sample aliquots were diluted with 1× PBS pH 3.0 and deposited onto precleaned silicon wafer. AFM-IR analysis was performed in contact mode. At least 30–40 individual aggregates were analyzed for each sample.

https://doi.org/10.1021/acsomega.3c00159
ACS Omega 2023, 8, 12379–12386

observe ester (1730 cm^{-1}) vibration in the spectra collected from Ins:PE. These findings show that Ins:PE possesses substantially less lipids in their structure and that the PE and PC have drastically different interactions with insulin in such oligomers. These conclusions are further supported by very intense vibrational bands around 1400 to 1580 cm^{-1}, which can be assigned to the C−H vibrations of lipids, observed in the AFM-IR spectra of Ins:PE and not evident in the spectrum of Ins:PC.

Ins:PE oligomers also exhibited both 1630 and 1668 cm^{-1} bands in their spectra with nearly similar intensities. This suggests that Ins:PE have both parallel β-sheets and unordered proteins present in their secondary structure. A similar pattern of 1630 and 1668 cm^{-1} bands was observed in the AFM-IR spectra collected from Ins:PG. This points to the similarity in their secondary structure with Ins:PE oligomers. At the same time, AFM-IR analysis of Ins:PS and Ins:CL fibrils shows that these aggregates are dominated by parallel β-sheets with some unordered proteins present in their secondary structure.[45,46] It should be noted that spectra collected from Ins:PS, Ins:PG, and Ins:CL exhibit strong vibrational bands at 800−900 cm^{-1} and 1000−1200 cm^{-1}, which indicates that phospholipids are present in their structure. Based on these results, we can conclude that the structure of insulin aggregates that were grown in the lipid-free environment is drastically different from the structure of insulin aggregates that were grown in the presence of lipids. We also found that all insulin aggregates that were grown in the presence of phospholipids possess lipids in their structure. Finally, from the perspective of protein secondary structure, all aggregates can be divided into three groups. (i) Aggregates dominated by parallel β-sheets that include Ins, Ins:PS, and Ins:CL; (ii) Aggregates with equal amounts of parallel β-sheets and unordered protein secondary structure that include Ins:PE and Ins:PG, and (iii) oligomers dominated by unordered protein secondary structure (Ins:PC).

Toxicity of Insulin Aggregates. We performed lactate dehydrogenase (LDH) assay to investigate the extent to which different protein aggregates exert toxicity to mice midbrain N27 cells (Figure 4).[33] We found that the toxicity of Ins:PC and Ins:PE was significantly lower than the toxicity exerted by Ins fibrils. Furthermore, we found that Ins:PC were far less toxic than Ins:PE. Ins:PG showed levels similar to Ins fibrils. However, Ins:PS were found to be far less toxic than Ins:PG. LDH results showed that Ins:PS toxicity was similar to the toxicity exerted by Ins:PC. Finally, Ins:CL aggregates were also significantly less toxic than Ins aggregates. Ins:CL toxicity was higher than the toxicity exerted by Ins:PC and Ins:PS, but lower than the toxicity of Ins:PE. These results show that the toxicity of insulin aggregates grown in the presence of lipids is determined by the chemical structure of the lipid rather than the charge present on its headgroup. This conclusion is further supported by observed differences in the toxicities of lipids themselves. Specifically, we found that PC, PS, and CL were not toxic to N27 cells, whereas PE and PG were toxic to the cells. It should be noted that toxicity of the corresponding protein aggregates (Ins:PE and Ins:PG) was significantly greater than the toxicity of these lipids themselves.

Amyloid aggregates exert toxicities by enhancing reactive oxygen species (ROS) production and inducing mitochondrial dysfunction in cells.[47,48] Therefore, we investigated the extent to which Ins:PC, Ins:PE, Ins:PG, Ins:PS, and Ins:CL, as well insulin fibrils grown in the lipid-free environment are engaged

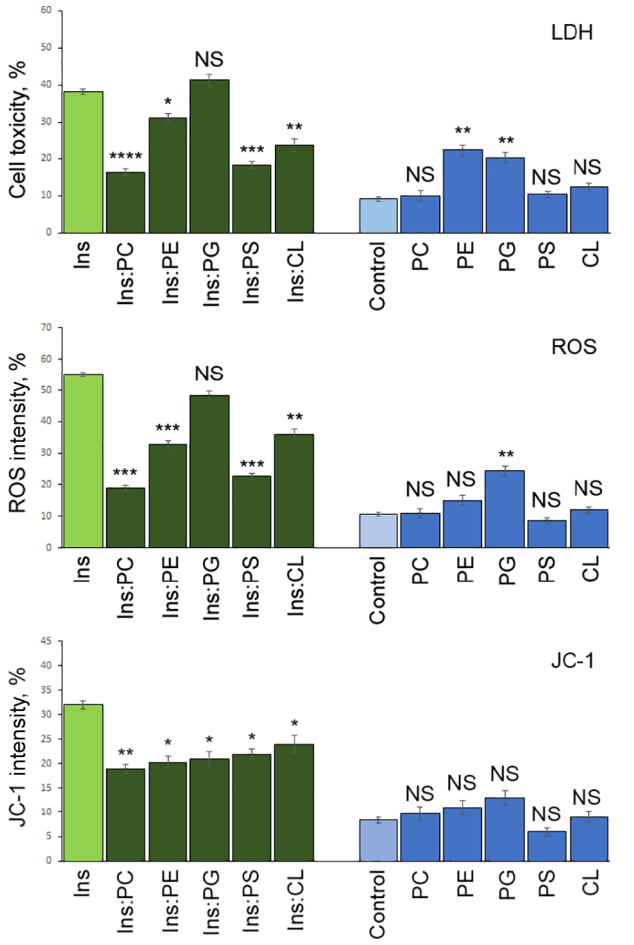

Figure 4. Toxicity of insulin aggregates grown in the presence of lipids is determined by the chemical structure of the lipid. Histograms of LDH (top), ROS (middle), and JC-1 (bottom) toxicity assays of Ins, Ins:PC, Ins:PE, Ins:PG, Ins:PS, and Ins:CL, as well as PC, PE, PG, PS, and CL. After 24 h of incubation of insulin (400 μM) with and without lipids at 37 °C under 510 rpm, sample triplicates were exposed to mice midbrain N27 cells for 48 h. For each of the presented results, three independent measurements were made.

in ROS production and mitochondrial dysfunction of mice midbrain N27 cells (Figure 4)7.

We found that ROS levels exerted by the insulin aggregates that were grown in the presence and absence of lipids are very similar to the LDH responses of N27 cells to these specimens. Specifically, Ins:PC and Ins:PS exerted the lowest compared to Ins levels of ROS. Ins:PE and Ins:CL induced significantly higher levels of ROS than Ins:PC, Ins:PS, and Ins. However, Ins:PG were found to exert comparable to Ins ROS levels in the N27 cell line. Thus, ROS levels are determined by the chemical structure of the lipid rather than the charge present on its headgroup. It should be noted that only PG was found to be significantly more toxic than control, whereas all other lipids were found to cause an insignificant increase in the ROS production.

From the analysis of the level of mitochondrial dysfunction caused by insulin aggregates that were grown in the presence and absence of lipids, one can conclude that Ins:PC, Ins:PE, Ins:PG, Ins:PS, and Ins:CL exert significantly lower levels than Ins levels of mitochondrial dysfunction. However, we found no differences in the levels of JC-1 intensity between insulin aggregates that were grown in the presence of lipids. Thus, the

https://doi.org/10.1021/acsomega.3c00159
ACS Omega 2023, 8, 12379−12386

presence of lipid allows for the minimization of the mitochondrial dysfunction caused by amyloid aggregates, however, the degree of the mitochondrial stress does not depend on the chemical structure of the lipid.

DISCUSSION

The abrupt aggregation of misfolded proteins in different organs and tissues is a hallmark of amyloid diseases, a large group of pathologies that include Alzheimer and Parkinson diseases.[14−16] In the postmortem detected deposits, proteins are assembled into long fibrils.[17,47] Using cryo-electron microscopy and solid-state nuclear magnetic resonance, secondary structures of the fibrils were resolved. It appeared that they have two β-sheets that are held together by hydrogen bonding.[49−51] These two β-sheets can intertwine and coil, which provides a twist to the mature fibrils. Alternatively, β-sheets can assemble side-by-side to each other, which results in tape-like flat topologies of mature amyloid fibrils.

A growing body of experimental evidence suggests that a large number of molecules and ions can alter protein aggregation, as well as modify the toxicity and secondary structure of fibrils.[48,52,53] For instance, Cataldi and co-workers found that 3,4-dihydroxyphenylacetaldehyde, a product of dopamine oxidation, could alter the secondary structure of amyloid β oligomers significantly increasing their toxicity.[48] Mannini and co-workers found that the presence of zinc ions in the solution of amyloid β peptides yields stable oligomers that exert high cell toxicity.

Lipids are a large class of biological molecules that perform a large number of physiologically important functions in cells.[1−4] Lipids are the major components of plasma and organelle membranes that determine membrane fluidity and permeability for molecules and ions. Lipids also act as secondary messengers in signal transduction across the plasma membrane.[54] It was recently reported that amyloid proteins can interact with lipids forming complexes that have enhanced hydrophobicity.[17] This allows for such amyloid:lipid structures to pass thorough the lipid bilayers into the cytosol, where they trigger ROS production and endoplasmic reticulum stress, ultimately causing cell death.[32−34,55−57]

Recently, Zhang and co-workers demonstrated that anionic lipids accelerated the aggregation of IAPP, whereas zwitterionic lipid did not alter the rate of protein aggregation.[58] Anionic lipids also enhanced the membrane permeabilization properties of IAPP aggregates, whereas this effect was not observed for zwitterionic lipids. These and other research findings suggest that the charge of the lipids can play a critically important role in protein aggregation and toxicity of the corresponding amyloid aggregates.[18,59,60]

Our results show that the charge of the phospholipid head determines the aggregation properties of insulin if the lipid is present in a 1:1 molar ratio with the protein. Specifically, zwitterionic PC and PE inhibit fibril formation, whereas negatively charged PS, PG, and CL strongly accelerate insulin aggregation. Furthermore, our results show that the charge of the phospholipid head determines the morphology of the protein aggregates formed in the lipid presence. Specifically, an exposition of insulin to PC and PE leads to the formation of small oligomers. However, in the presence of PS, PG, and CL, short fibril aggregates that are drastically different from long fibrils formed by insulin in the lipid-free environment. It should be noted that the exact value of the lipid charge (−1 vs −2) has only a minor if any effect on the topology of the protein aggregates formed in the presence of lipids. Specifically, we found that morphologies of Ins:PG and Ins:PS aggregates were very similar to the topology of Ins:CL fibrils.

Examination of the secondary structure of insulin aggregates that were grown in the presence of lipids did not reveal a clear correlation between the morphology of the aggregates and their structural organization. We found that Ins:PC oligomers are dominated by unordered proteins, whereas Ins:PE oligomers have nearly equal contributions of unordered proteins and parallel β-sheets in their secondary structure. AFM-IR showed that a similar secondary structure was evident for Ins:PG fibrils. Thus, structurally different oligomers can be formed in the presence of different zwitterionic lipids. The same conclusions can be extended to the fibrils formed by negatively charged lipids. Specifically, the secondary structures of Ins:PS and Ins:CL were found to be very similar, however, significantly different from the secondary structure of Ins:PG. These findings suggest that the secondary structure is determined by the chemical structure of the lipid rather than by the charge of the phospholipid polar head.

AFM-IR revealed that Ins:PC, Ins:PE, Ins:PS, Ins:PG, and Ins:CL aggregates contained the corresponding lipids in their structure. Furthermore, LDH results showed that PG and PE were found to be significantly toxic to the cells, whereas PC, PG, and CL exerted no cell toxicity. We also observed that the toxicity of Ins:PG and Ins:PE was significantly higher than the toxicity exerted by Ins:PC, Ins:PS, and Ins:CL. These results show that the toxicity of insulin aggregates is determined by the chemical structure of the lipid present in their structure. Consequently, not the charge of the phospholipid polar head but the chemical structure of the lipid determines the toxicity of the amyloid aggregates formed in the presence of these lipids.

These results help to understand the abundance of PC and PE in the plasma membrane. One can imagine that these lipids form complexes with amyloid-associated proteins such as insulin lowering their aggregation properties. At the same time, the presence of negatively charged lipids, such as PS, facilitates the abrupt aggregation of insulin. It is known that PS is primarily localized on the cytosolic part of the plasma membrane. Its appearance on the exterior part is indicative of cell malfunction. In such cases, PS is recognized by macrophages that eliminate such preapoptotic cells. Expanding upon this, one can envision that an age-related delay in the clearance of preapoptotic cells may increase the possibility of abrupt aggregation of amyloid proteins on their PS-rich plasma membranes. Highly likely, similar molecular mechanisms can enable the appearance of CL on the exterior part of mitochondria that enhance the aggregation properties of the intracellular proteins.

Once formed on the surface of plasma or mitochondrial membranes, amyloid aggregates can directly enter the cell or organelles permeabilizing their membranes.[61] Alternatively, amyloid aggregates can be taken up by endocytosis. Matveyenka and co-workers recently demonstrated that in such cases, amyloid aggregates could damage cell endosomes which allowed for their escape in the cell cytosol.[34] In this case, endosomal damage is followed by enhanced ROS levels and mitochondrial damage that ultimately led to cell death.[34,54] Matveyenka and co-workers also found that amyloid aggregates caused significant damage of cell endoplasmic reticulum via the activation of unfolded protein response.[62] These results demonstrate that amyloid-induced cell death can involve

https://doi.org/10.1021/acsomega.3c00159
ACS Omega 2023, 8, 12379−12386

multiple molecular mechanisms. Thus, additional studies are required to fully elucidate mechanisms responsible for amyloid-induce cell death.[63]

CONCLUSIONS

Our results point to the direct correlation between the rate of insulin aggregation and the charge of the phospholipid head. Specifically, zwitterions strongly inhibited fibril formation, whereas negatively charged PS, CL, and PG accelerated insulin aggregation. We also found a direct relationship between the charge of the phospholipid head and the morphology of the protein aggregates formed in the presence of lipids. Specifically, in the presence of PC and PE, we found only small oligomers. However, in the presence of negatively charged phospholipids, short fibril-like aggregates were observed. It should be noted that in the lipid-free environment, insulin yielded drastically different fibrils compared to those formed in the presence of lipids. From the analysis of the secondary structure and toxicity exerted by Ins:PC, Ins:PE, Ins:PS, and Ins:PG, we found that the secondary structure and toxicity are determined by the chemical structure of the lipid rather than by the charge of the phospholipid polar head.

EXPERIMENTAL SECTION

Materials. Bovine insulin was purchased from Sigma-Aldrich (St. Louis, MO, USA); 1,2-dimyristoyl-sn-glycero-3-phospho-L-serine (DMPS or PS) 1,2-dimyristoyl-sn-glycero-3-phosphocholine (DMPC or PC), 1,2-dimyristoyl-sn-glycero-3-phosphoethanolamine (DMPE or PE), 1,2-dimyristoyl-sn-glycero-3-phospho(1′-rac glycerol) (DMPG or PG), and 1′,3′-bis[1,2-distearoyl-sn-glycero-3-phospho]-glycerol (18:0 CL) were purchased from Avanti (Alabaster, AL, USA).

Liposome Preparation. To make large unilamellar vesicles (LUVs) of phospholipids, 0.6 mg of each lipid were first dissolved in 2.6 mL of PBS pH 7.4. Right after, solutions were heated to ∼50 °C in a water bath for approximately 30 min. Next, lipid solutions were immersed into liquid nitrogen and kept there for ∼5 min. The thawing−freezing cycle was repeated 10 times. Finally, to even better unify the size of LUVs, lipid solutions were passed 15 times through a 100 nm membrane installed in the extruder (Avanti, Alabaster, AL, USA). Dynamic light scattering was utilized to ensure that the size of LUVs was 100 nm ± 10 nm prior to any experiment.

Insulin Aggregation. We dissolved 200 μM of insulin in BPS adjusting pH to 3.0 using concentrated hydrochloric acid (HCl). In parallel, 200 μM of insulin was mixed with the equivalent concentration of lipids. Using concentrated HCl, pH of lipid-protein solutions was adjusted to pH 3.0. Samples were placed into a 96 well-plate and indicated in the plate reader (Tecan, Männedorf, Switzerland) at 37 °C under 510 rpm for 24 h.

Kinetic Measurements. Thioflavin T (ThT) assay was used to monitor the rate of insulin aggregation For this, protein and protein-lipid samples were mixed with 2 mM of ThT solution. Samples were placed into a 96 well-plate and indicated in the plate reader (Tecan, Männedorf, Switzerland) at 37 °C under 510 rpm for 24 h. Fluorescence measurements were taken every 10 min with 450 nm excitation; emission was acquired at 488 nm.

AFM Imaging. Microscopic analysis of protein aggregates formed after 24 h of sample invitation at 37 °C under 510 rpm shaking was performed on the AIST-NT-HORIBA system (Edison, NJ). For sample imaging, tapping mode AFM probes (Appnano (Mountain View, CA, USA)) were used. To prepare the sample, we diluted an aliquot of the sample in 1× PBS, pH 3.0. This protein suspension was placed onto precleaned silicon wafer and was kept on it for 1−20 min. Next, excess of the suspension was removed from the silicon surface; wafer was dried under a flow of dry nitrogen. Imaging analysis was performed using AIST-NT software (Edison, NJ, USA).

AFM-IR. To acquire AFM-IR spectra, we used a Nano-IR3 system (Bruker, Santa Barbara, CA, USA). Contact-mode AFM tips (ContGB-G AFM probe, NanoAndMore, Watsonville, CA, USA) were used. Sample preparation was identical to that of the above discussed AFM imaging.

Cell Toxicity Assays. We used mice midbrain N27 cells to examine the toxicity of insulin aggregates. For this, cells were grown in RPMI 1640 medium (Thermo Fisher Scientific, Waltham, MA, USA) with added 10% fetal bovine serum (FBS) (Invitrogen, Waltham, MA, USA). Cells were kept in a 96 well-plate (5000 cells per well) at 37 °C under 5% CO_2. Once ∼70% confluency was observed, 100 μL of the cell culture was replaced with 100 μL RPMI 1640 medium containing 5% FBS containing protein samples. Cells with protein aggregates were incubated for 48 h. After that, LDH assay was performed using CytoTox 96 nonradioactive cytotoxicity assay (G1781, Promega, Madison, WI, USA). A Tecan plate reader (Männedorf, Switzerland) was used to acquire the absorption of the solutions at 490 nm. Every well was measured 25 times in different locations. All measurements were made in triplicate. We used T-test to investigate the statistical significance of differences between the toxicity of analyzed samples.

The same cells were used to perform ROS assay. For this, an ROS reagent (C10422, Invitrogen, Waltham, MA, USA) was added to the cells to the final concentration of 5 μM. Cells with the reagent were incubated at 37 °C under 5% CO_2 for 30 min. Next, the supernatant was removed, and cells were washed with PBS. Finally, cells were resuspended in 200 μL of PBS.

For JC-1 assay, 1 μL of JC-1 reagent (M34152A, Invitrogen, Waltham, MA, USA) was added to N27 cells. Cells were incubated with the reagent at 37 °C under 5% CO_2 for 30 min. Next, the supernatant was removed, and cells were washed with PBS. LSR II Flow Cytometer (BD, San Jose, CA, USA) was used to process the cells using red channel (λ = 633 nm). LSR II software was used to calculate the percentages of mitochondrial damage in cells.

AUTHOR INFORMATION

Corresponding Author

Dmitry Kurouski − *Department of Biochemistry and Biophysics and Department of Biomedical Engineering, Texas A&M University, College Station, Texas 77843, United States;* orcid.org/0000-0002-6040-4213; Phone: 979-458-3778; Email: dkurouski@tamu.edu

Authors

Mikhail Matveyenka − *Department of Biochemistry and Biophysics, Texas A&M University, College Station, Texas 77843, United States*

Stanislav Rizevsky − *Department of Biochemistry and Biophysics, Texas A&M University, College Station, Texas 77843, United States; Department of Biotechnology, Binh Duong University, Thu Dau Mot 820000, Vietnam*

https://doi.org/10.1021/acsomega.3c00159
ACS Omega 2023, 8, 12379−12386

Complete contact information is available at:
https://pubs.acs.org/10.1021/acsomega.3c00159

Author Contributions

[‖]M.M. and S.R. contributed equally to this study.

Notes

The authors declare no competing financial interest.

■ ACKNOWLEDGMENTS

We are grateful to the National Institute of Health for providing financial support (R35GM142869).

■ REFERENCES

(1) van Meer, G.; Voelker, D. R.; Feigenson, G. W. Membrane lipids: where they are and how they behave. *Nat. Rev. Mol. Cell Biol.* **2008**, *9*, 112−124.
(2) Fahy, E.; Subramaniam, S.; Murphy, R. C.; Nishijima, M.; Raetz, C. R.; Shimizu, T.; Spener, F.; van Meer, G.; Wakelam, M. J.; Dennis, E. A. Update of the LIPID MAPS comprehensive classification system for lipids. *J. Lipid Res.* **2009**, *50*, S9−S14.
(3) Fitzner, D.; Bader, J. M.; Penkert, H.; Bergner, C. G.; Su, M.; Weil, M. T.; Surma, M. A.; Mann, M.; Klose, C.; Simons, M. Cell-Type- and Brain-Region-Resolved Mouse Brain Lipidome. *Cell Rep.* **2020**, *32*, No. 108132.
(4) Michaelson, D. M.; Barkai, G.; Barenholz, Y. Asymmetry of lipid organization in cholinergic synaptic vesicle membranes. *Biochem. J.* **1983**, *211*, 155−162.
(5) Pope, S.; Land, J. M.; Heales, S. J. R. Oxidative stress and mitochondrial dysfunction in neurodegeneration; cardiolipin a critical target? *Biochim. Biophys. Acta* **2008**, *1777*, 794−799.
(6) Falabella, M.; Vernon, H. J.; Hanna, M. G.; Claypool, S. M.; Pitceathly, R. D. S. Cardiolipin, Mitochondria, and Neurological Disease. *Trends Endocrinol. Metab.* **2021**, *32*, 224−237.
(7) Stace, C. L.; Ktistakis, N. T. Phosphatidic acid- and phosphatidylserine-binding proteins. *Biochim. Biophys. Acta* **2006**, *1761*, 913−926.
(8) Mizuno, S.; Sasai, H.; Kume, A.; Takahashi, D.; Satoh, M.; Kado, S.; Sakane, F. Dioleoyl-phosphatidic acid selectively binds to alpha-synuclein and strongly induces its aggregation. *FEBS Lett.* **2017**, *591*, 784−791.
(9) Levental, I.; Levental, K. R.; Heberle, F. A. Lipid Rafts: Controversies Resolved, Mysteries Remain. *Trends Cell. Biol.* **2020**, *30*, 341−353.
(10) Alecu, I.; Bennett, S. A. L. Dysregulated Lipid Metabolism and Its Role in alpha-Synucleinopathy in Parkinson's Disease. *Front. Neurosci.* **2019**, *13*, 328.
(11) Banerjee, S.; Sun, Z.; Hayden, E. Y.; Teplow, D. B.; Lyubchenko, Y. L. Nanoscale Dynamics of Amyloid beta-42 Oligomers As Revealed by High-Speed Atomic Force Microscopy. *ACS Nano* **2017**, *11*, 12202−12209.
(12) Zhang, Y.; Hashemi, M.; Lv, Z.; Williams, B.; Popov, K. I.; Dokholyan, N. V.; Lyubchenko, Y. L. High-speed atomic force microscopy reveals structural dynamics of alpha-synuclein monomers and dimers. *J. Chem. Phys.* **2018**, *148*, No. 123322.
(13) Kakinen, A.; Xing, Y.; Hegoda Arachchi, N.; Javed, I.; Feng, L.; Faridi, A.; Douek, A. M.; Sun, Y.; Kaslin, J.; Davis, T. P.; Higgins, M. J.; Ding, F.; Ke, P. C. Single-Molecular Heteroamyloidosis of Human Islet Amyloid Polypeptide. *Nano Lett.* **2019**, *19*, 6535−6546.
(14) Chiti, F.; Dobson, C. M. Protein Misfolding, Amyloid Formation, and Human Disease: A Summary of Progress Over the Last Decade. *Annu. Rev. Biochem.* **2017**, *86*, 27−68.
(15) Knowles, T. P. J.; Vendruscolo, M.; Dobson, C. M. The amyloid state and its association with protein misfolding diseases. *Nat. Rev. Mol. Cell Biol.* **2014**, *15*, 384−396.
(16) Iadanza, M. G.; Jackson, M. P.; Hewitt, E. W.; Ranson, N. A.; Radford, S. E. A new era for understanding amyloid structures and disease. *Nat. Rev. Mol. Cell Biol.* **2018**, *19*, 755−773.
(17) Dou, T.; Zhou, L.; Kurouski, D. Unravelling the Structural Organization of Individual alpha-Synuclein Oligomers Grown in the Presence of Phospholipids. *J. Phys. Chem. Lett.* **2021**, *12*, 4407−4414.
(18) Rizevsky, S.; Matveyenka, M.; Kurouski, D. Nanoscale Structural Analysis of a Lipid-Driven Aggregation of Insulin. *J. Phys. Chem. Lett.* **2022**, *13*, 2467−2473.
(19) Rizevsky, S.; Zhaliazka, K.; Dou, T.; Matveyenka, M.; Kurouski, D. Characterization of Substrates and Surface-Enhancement in Atomic Force Microscopy Infrared Analysis of Amyloid Aggregates. *J. Phys. Chem. C Nanomater. Interfaces* **2022**, *126*, 4157−4162.
(20) Dazzi, A.; Glotin, F.; Carminati, R. Theory of infrared nanospectroscopy by photothermal induced resonance. *J. Appl. Phys.* **2010**, *107*, No. 124519.
(21) Dazzi, A.; Prater, C. B. AFM-IR: Technology and Applications in Nanoscale Infrared Spectroscopy and Chemical Imaging. *Chem. Rev.* **2017**, *117*, 5146−5173.
(22) Centrone, A. Infrared imaging and spectroscopy beyond the diffraction limit. *Annu. Rev. Anal. Chem.* **2015**, *8*, 101−126.
(23) Chae, J.; An, S.; Ramer, G.; Stavila, V.; Holland, G.; Yoon, Y.; Talin, A. A.; Allendorf, M.; Aksyuk, V. A.; Centrone, A. Nanophotonic Atomic Force Microscope Transducers Enable Chemical Composition and Thermal Conductivity Measurements at the Nanoscale. *Nano Lett.* **2017**, *17*, 5587−5594.
(24) Kurouski, D.; Dazzi, A.; Zenobi, R.; Centrone, A. Infrared and Raman chemical imaging and spectroscopy at the nanoscale. *Chem. Soc. Rev.* **2020**, *49*, 3315−3347.
(25) Ramer, G.; Aksyuk, V. A.; Centrone, A. Quantitative Chemical Analysis at the Nanoscale Using the Photothermal Induced Resonance Technique. *Anal. Chem.* **2017**, *89*, 13524−13531.
(26) Ruggeri, F. S.; Benedetti, F.; Knowles, T. P. J.; Lashuel, H. A.; Sekatskii, S.; Dietler, G. Identification and nanomechanical characterization of the fundamental single-strand protofilaments of amyloid alpha-synuclein fibrils. *Proc. Natl. Acad. Sci. U. S. A.* **2018**, *115*, 7230−7235.
(27) Ruggeri, F. S.; Charmet, J.; Kartanas, T.; Peter, Q.; Chia, S.; Habchi, J.; Dobson, C. M.; Vendruscolo, M.; Knowles, T. P. J. Microfluidic deposition for resolving single-molecule protein architecture and heterogeneity. *Nat. Commun.* **2018**, *9*, 3890.
(28) Ruggeri, F. S.; Flagmeier, P.; Kumita, J. R.; Meisl, G.; Chirgadze, D. Y.; Bongiovanni, M. N.; Knowles, T. P. J.; Dobson, C. M. The Influence of Pathogenic Mutations in alpha-Synuclein on Biophysical and Structural Characteristics of Amyloid Fibrils. *ACS Nano* **2020**, *14*, 5213−5222.
(29) Ruggeri, F. S.; Longo, G.; Faggiano, S.; Lipiec, E.; Pastore, A.; Dietler, G. Infrared nanospectroscopy characterization of oligomeric and fibrillar aggregates during amyloid formation. *Nat. Commun.* **2015**, *6*, 7831.
(30) Ruggeri, F. S.; Mannini, B.; Schmid, R.; Vendruscolo, M.; Knowles, T. P. J. Single molecule secondary structure determination of proteins through infrared absorption nanospectroscopy. *Nat. Commun.* **2020**, *11*, 2945.
(31) Ruggeri, F. S.; Vieweg, S.; Cendrowska, U.; Longo, G.; Chiki, A.; Lashuel, H. A.; Dietler, G. Nanoscale studies link amyloid maturity with polyglutamine diseases onset. *Sci. Rep.* **2016**, *6*, 31155.
(32) Matveyenka, M.; Rizevsky, S.; Kurouski, D. Unsaturation in the Fatty Acids of Phospholipids Drastically Alters the Structure and Toxicity of Insulin Aggregates Grown in Their Presence. *J. Phys. Chem. Lett.* **2022**, *13*, 4563−4569.
(33) Matveyenka, M.; Rizevsky, S.; Kurouski, D. The degree of unsaturation of fatty acids in phosphatidylserine alters the rate of insulin aggregation and the structure and toxicity of amyloid aggregates. *FEBS Lett.* **2022**, *596*, 1424−1433.
(34) Matveyenka, M.; Rizevsky, S.; Pellois, J. P.; Kurouski, D. Lipids uniquely alter rates of insulin aggregation and lower toxicity of amyloid aggregates. *Biochim. Biophys. Acta Mol. Cell Biol. Lipids* **2023**, *1868*, No. 159247.
(35) Zhaliazka, K.; Rizevsky, S.; Matveyenka, M.; Serada, V.; Kurouski, D. Charge of Phospholipids Determines the Rate of

Lysozyme Aggregation but Not the Structure and Toxicity of Amyloid Aggregates. *J. Phys. Chem. Lett.* **2022**, *13*, 8833−8839.
(36) Zhaliazka, K.; Kurouski, D. Nanoscale Characterization of Parallel and Antiparallel beta-Sheet Amyloid Beta 1-42 Aggregates. *ACS Chem. Neurosci.* **2022**, *13*, 2813−2820.
(37) Zhaliazka, K.; Matveyenka, M.; Kurouski, D. Lipids Uniquely Alter the Secondary Structure and Toxicity of Amyloid beta 1-42 Aggregates. *FEBS J.* **2023**, in press , DOI: 10.1111/febs.16738.
(38) Gupta, Y.; Singla, G.; Singla, R. Insulin-derived amyloidosis. *Indian J. Endocrinol. Metab.* **2015**, *19*, 174−177.
(39) Shikama, Y.; Kitazawa, J.; Yagihashi, N.; Uehara, O.; Murata, Y.; Yajima, N.; Wada, R.; Yagihashi, S. Localized amyloidosis at the site of repeated insulin injection in a diabetic patient. *Intern. Med.* **2010**, *49*, 397−401.
(40) Iwaya, K.; Zako, T.; Fukunaga, J.; Sörgjerd, K. M.; Ogata, K.; Kogure, K.; Kosano, H.; Noritake, M.; Maeda, M.; Ando, Y.; Katsura, Y.; Nagase, T. Toxicity of insulin-derived amyloidosis: a case report. *BMC Endocr. Disord.* **2019**, *19*, 61.
(41) D'Souza, A.; Theis, J. D.; Vrana, J. A.; Buadi, F.; Dispenzieri, A.; Dogan, A. Localized insulin-derived amyloidosis: a potential pitfall in the diagnosis of systemic amyloidosis by fat aspirate. *Am. J. Hematol.* **2012**, *87*, E131−E132.
(42) Katzenmeyer, A. M.; Aksyuk, V.; Centrone, A. Nanoscale infrared spectroscopy: improving the spectral range of the photothermal induced resonance technique. *Anal. Chem.* **2013**, *85*, 1972−1979.
(43) Katzenmeyer, A. M.; Holland, G.; Kjoller, K.; Centrone, A. Absorption spectroscopy and imaging from the visible through mid-infrared with 20 nm resolution. *Anal. Chem.* **2015**, *87*, 3154−3159.
(44) Dou, T.; Li, Z.; Zhang, J.; Evilevitch, A.; Kurouski, D. Nanoscale Structural Characterization of Individual Viral Particles Using Atomic Force Microscopy Infrared Spectroscopy (AFM-IR) and Tip-Enhanced Raman Spectroscopy (TERS). *Anal. Chem.* **2020**, *92*, 11297−11304.
(45) Kurouski, D.; Lombardi, R. A.; Dukor, R. K.; Lednev, I. K.; Nafie, L. A. Direct observation and pH control of reversed supramolecular chirality in insulin fibrils by vibrational circular dichroism. *Chem. Commun.* **2010**, *46*, 7154−7156.
(46) Sarroukh, R.; Goormaghtigh, E.; Ruysschaert, J. M.; Raussens, V. ATR-FTIR: a ″rejuvenated″ tool to investigate amyloid proteins. *Biochim. Biophys. Acta* **2013**, *1828*, 2328−2338.
(47) Chen, S. W.; Drakulic, S.; Deas, E.; Ouberai, M.; Aprile, F. A.; Arranz, R.; Ness, S.; Roodveldt, C.; Guilliams, T.; De-Genst, E. J.; Klenerman, D.; Wood, N. W.; Knowles, T. P.; Alfonso, C.; Rivas, G.; Abramov, A. Y.; Valpuesta, J. M.; Dobson, C. M.; Cremades, N. Structural characterization of toxic oligomers that are kinetically trapped during alpha-synuclein fibril formation. *Proc. Natl. Acad. Sci. U. S. A.* **2015**, *112*, E1994−E2003.
(48) Cataldi, R.; Chia, S.; Pisani, K.; Ruggeri, F. S.; Xu, C. K.; Sneideris, T.; Perni, M.; Sarwat, S.; Joshi, P.; Kumita, J. R.; Linse, S.; Habchi, J.; Knowles, T. P. J.; Mannini, B.; Dobson, C. M.; Vendruscolo, M. A dopamine metabolite stabilizes neurotoxic amyloid-beta oligomers. *Commun. Biol.* **2021**, *4*, 19.
(49) Li, B.; Ge, P.; Murray, K. A.; Sheth, P.; Zhang, M.; Nair, G.; Sawaya, M. R.; Shin, W. S.; Boyer, D. R.; Ye, S.; Eisenberg, D. S.; Zhou, Z. H.; Jiang, L. Cryo-EM of full-length alpha-synuclein reveals fibril polymorphs with a common structural kernel. *Nat. Commun.* **2018**, *9*, 3609.
(50) Guerrero-Ferreira, R.; Taylor, N. M.; Mona, D.; Ringler, P.; Lauer, M. E.; Riek, R.; Britschgi, M.; Stahlberg, H. Cryo-EM structure of alpha-synuclein fibrils. *Elife* **2018**, *7*, No. e36402.
(51) Tycko, R. Solid-state NMR studies of amyloid fibril structure. *Annu. Rev. Phys. Chem.* **2011**, *62*, 279−299.
(52) Vosough, F.; Barth, A. Characterization of Homogeneous and Heterogeneous Amyloid-beta42 Oligomer Preparations with Biochemical Methods and Infrared Spectroscopy Reveals a Correlation between Infrared Spectrum and Oligomer Size. *ACS Chem. Neurosci.* **2021**, *12*, 473−488.
(53) Jinsmaa, Y.; Sullivan, P.; Sharabi, Y.; Goldstein, D. S. DOPAL is transmissible to and oligomerizes alpha-synuclein in human glial cells. *Auton. Neurosci.* **2016**, *194*, 46−51.
(54) Matveyenka, M.; Zhaliazka, K.; Rizevsky, S.; Kurouski, D. Lipids uniquely alter secondary structure and toxicity of lysozyme aggregates. *FASEB J.* **2022**, *36*, No. e22543.
(55) Alza, N. P.; Iglesias Gonzalez, P. A.; Conde, M. A.; Uranga, R. M.; Salvador, G. A. Lipids at the Crossroad of alpha-Synuclein Function and Dysfunction: Biological and Pathological Implications. *Front. Cell Neurosci.* **2019**, *13*, 175.
(56) Galvagnion, C. The Role of Lipids Interacting with -Synuclein in the Pathogenesis of Parkinson's Disease. *J. Parkins. Dis.* **2017**, *7*, 433−450.
(57) Galvagnion, C.; Brown, J. W. P.; Ouberai, M. M.; Flagmeier, P.; Vendruscolo, M.; Buell, A. K.; Sparr, E.; Dobson, C. M. Chemical properties of lipids strongly affect the kinetics of the membrane-induced aggregation of alpha-synuclein. *Proc. Natl. Acad. Sci. U. S. A.* **2016**, *113*, 7065−7070.
(58) Zhang, X.; St Clair, J. R.; London, E.; Raleigh, D. P. Islet Amyloid Polypeptide Membrane Interactions: Effects of Membrane Composition. *Biochemistry* **2017**, *56*, 376−390.
(59) Matveyenka, M.; Rizevsky, S.; Kurouski, D. Length and Unsaturation of Fatty Acids of Phosphatidic Acid Determines the Aggregation Rate of Insulin and Modifies the Structure and Toxicity of Insulin Aggregates. *ACS Chem. Neurosci.* **2022**, *13*, 2483−2489.
(60) Rizevsky, S.; Zhaliazka, K.; Matveyenka, M.; Quinn, K.; Kurouski, D. Lipids reverse supramolecular chirality and reduce toxicity of amyloid fibrils. *FEBS J.* **2022**, *289*, 7537−7544.
(61) Srinivasan, S.; Patke, S.; Wang, Y.; Ye, Z.; Litt, J.; Srivastava, S. K.; Lopez, M. M.; Kurouski, D.; Lednev, I. K.; Kane, R. S.; Colon, W. Pathogenic serum amyloid A 1.1 shows a long oligomer-rich fibrillation lag phase contrary to the highly amyloidogenic non-pathogenic SAA2.2. *J. Biol. Chem.* **2013**, *288*, 2744−2755.
(62) Matveyenka, M.; Rizevsky, S.; Kurouski, D. Amyloid aggregates exert cell toxicity causing irreversible damages in the endoplasmic reticulum. *Biochim. Biophys. Acta Mol. Basis Dis.* **2022**, *1868*, No. 166485.
(63) Galvagnion, C.; Buell, A. K.; Meisl, G.; Michaels, T. C. T.; Vendruscolo, M.; Knowles, T. P. J.; Dobson, C. M. Lipid vesicles trigger α-synuclein aggregation by stimulating primary nucleation. *Nat. Chem. Biol.* **2015**, *11*, 229−234.

https://doi.org/10.1021/acsomega.3c00159
ACS Omega 2023, 8, 12379−12386